Hindawi Publishing Corporation
International Journal of Photoenergy
Volume 2013, Article ID 173760, 10 pages
http://dx.doi.org/10.1155/2013/173760

Research Article

Photoelectrocatalytic Performances of Nanostructured/Decorated TiO_2 Electrodes: Effect of Wavelength and Cell Configuration

Simonetta Palmas,[1] Michele Mascia,[1] Annalisa Vacca,[1] and Ilenia Tredici[2]

[1] *Dipartimento di Ingegneria Meccanica Chimica e dei Materiali, Università degli Studi di Cagliari, Via Marengo 2, 09123 Cagliari, Italy*
[2] *Dipartimento di Chimica, Università degli Studi di Pavia, Via Taramelli 12, 27100 Pavia, Italy*

Correspondence should be addressed to Simonetta Palmas; sipalmas@dicm.unica.it

Received 1 August 2013; Revised 20 November 2013; Accepted 20 November 2013

Academic Editor: Mahmoud M. El-Nahass

The behaviour of TiO_2 based electrodes was investigated during the photoelectrocatalytic water splitting process. TiO_2 nanotubes and compact oxide structures were obtained by electrochemical oxidation of Ti foils. A subsequent hydrothermal process carried out at both the nanotubular and compact oxide structures allowed decorating the structure by TiO_2 nanoparticles. The synthesized TiO_2 samples worked as photoanodes both in a bulk three electrode cell and in a thin gap cell. The results from measurements of the photocurrent and from electrochemical impedance spectroscopy were used to highlight a combined effect of the wavelength of the incident light and the kind of cell configuration, on the global performance of the systems. The results indicate that the decoration process does not result only in a simple increase of the specific surface, but it also determines a different concentration of the bulk and superficial sites in the electrode. The different response of the sites at different wavelengths, along with the accessibility of the electrolyte to the porous structure are evocated to justify the experimental behaviour observed.

1. Introduction

Hydrogen can be produced from various sources and by several methods. Among the others, photoelectrochemical (PEC) decomposition of water into hydrogen and oxygen may be considered as one of the most promising and eco-friendly methods. A PEC cell consists of a semiconductor electrode and a metal counter electrode immersed in an aqueous electrolyte. As the light hits the semiconductor surface, the electrode absorbs part of the light and generates electron-hole pairs. These electron-hole pairs react with water and split its molecule into hydrogen and oxygen [1].

One of the main points, which affect the global efficiency of the process, is the recombination of the photogenerated charges. Depending on the electron-activity of the material and on the capability of the electrolyte to interact with the holes, the rate of displacement of the electrons towards the external circuit, as well as the rate of oxidation of the electrolyte, may be so high that recombination is limited. On the contrary, when these conditions are not fulfilled the global efficiency of the process may be heavily affected.

The semiconductor material may be considered the most important part of the PEC cell. As it is well known, several factors including size, specific surface area, pore volume, pore structure, crystalline phase, and the exposed surface facets may be determinant on the photocatalytic performance of a semiconductor [2]. Therefore, the electronics of the semiconductor material, its morphology, and the specific method used to perform its synthesis assume a particular relevance.

Among the different semiconductors tested to date, TiO_2 is still one of the most attractive photocatalyst because of its appropriate electronic band structure, photostability, chemical inertness, and commercial availability. A huge number of papers appeared in the literature on the synthesis of TiO_2 nano- or microstructures with different morphologies and properties [3–5], always addressing the synthesis to obtain a high superficial area: spheres [6], nanorods [7], fibers [8],

tubes [9–13], sheets [14] have been fabricated. In addition, decorated and hierarchical architectures have been proposed [15–19]. According to the definition of Lee [20], the "hierarchical structures" consist of micrometer or nanometer-scale structures, formed by the aggregation of nanostructured low-dimensional elements. Several strategies, such as template-sacrificial techniques [21], hydrothermal [22], and electrochemical processes [23], have been employed for the fabrication of hierarchical TiO_2 morphologies. Moreover, the combination of different techniques of synthesis has been also used to obtain mixed nanometric structures [24]. Hollow structures, usually consisting of spherical structures derived from the organization of nanoparticles [25, 26], and dendritic structures, arising from the organization of nanofibers or nanotubes [20], are generally identified as possible routes to maximize both the surface/volume ratio of the material and the actual availability of surfaces. This fact may be one of the reasons for the increased performance of this kind of structures, when they are used as photocatalysts [27]. Another approach to improve the photoactivity of titania nanometric structures is the decoration with electron acceptors like noble metals [28, 29] or metal oxide nanoparticles which have been proved to increase the active surface area. Also the decoration of TiO_2 nanostructures with the deposition of titania nanoparticles can be used to enhance the roughness of the material [30]. Decoration of nanotubular TiO_2 structures with anatase nanowires has been recently proposed [31]: the decoration process induced a great enhancement of the interfacial area of the tubular structure.

The experimental work presented in this paper can be inserted in this framework. Investigation on TiO_2 nanostructured materials started in our laboratory since some years ago: firstly, the behaviour of the TiO_2 samples was investigated when they were used as anode in a three electrode bulk cell, during the process of photoelectrochemical water splitting. The attention was always paid on nanometric structures: since heterogeneous reactions are involved, so high superficial extent is always of great concern. Our study started considering particulated electrodes based on TiO_2 powder obtained by means of a ball milling process by which nanostructured particles were obtained [32]. Then nanotubular structures of TiO_2 have been synthetized electrochemically, since this kind of morphology is more indicated to favour a fast path for the electrons [33, 34].

In the present paper we focus on the preparation and characterisation of electrodes obtained by combining electrochemical and chemical techniques: titania nanotubes have been fabricated by anodization and subsequently decorated with TiO_2 nanoparticles employing an hydrothermal treatment. The electrophotocatalytic performances of the samples have been investigated at different wavelengths of the irradiating light. Moreover, attention is paid in this case on the effect of the cell configuration on the global performance of the system. In particular the decorated nanotubes have been characterized by photocurrent tests and electrochemical impedance spectroscopies (EIS) and used as anode in a simple three-electrochemical cell configuration (BC). The samples have been also tested in a two electrodes thin gap cell configuration (TGC): this kind of configuration can limit the ohmic and diffusive resistances arising during the photoelectrochemical process since TGC is characterised by a distance between electrodes in the order of 25–500 μm, which is a value not significantly larger than the Nernst diffusion layer [35]. The results of the present work allowed interpreting the singular combined effect of the light wavelength and of the cell configuration on the photocurrents.

2. Experimental

2.1. Preparation of the TiO_2 Electrodes. All the samples were obtained from Ti foils (0.25 mm thick, 99.7% metal basis, Aldrich). A preliminary treatment was performed in which Ti foils were degreased by sonication in acetone, then in isopropanol, and finally in methanol; they were then rinsed with deionized water and dried in a Nitrogen stream. To obtain the nanotubular TiO_2 electrodes (NT), after this preliminary treatment the Ti foils were electrochemically oxidised at 20 V in a glycerol solution (25% H_2O) + 0.14 M NaF for three hours. Then, the samples were annealed 3 h at 400°C in air.

The nanotubular decorated electrodes (NTD) were obtained by a hydrothermal treatment: the nanotubular substrates were immersed in a bottle with diluted HCl solution under stirring for 20 min at room temperature. A Ti precursor (Ti isopropoxide) was added dropwise to the mixture and stirred for 1 h. The bottle was then sealed and heated at temperatures ranging from 80 to 140°C for different times, under slight stirring. After the reaction, the substrates were rinsed with distilled water and ethanol and annealed at 400°C.

The compact oxides (OC) and the decorated compact oxide (OCD) electrodes were prepared with the same procedures described above, but without fluorides in the oxidation bath.

The four kinds of samples will be referred in the rest of the text as NT (TiO_2 nanotubes), NTD (TiO_2 nanotubes decorated), OC (compact TiO_2 oxide), and OCD (compact TiO_2 oxide decorated).

2.2. Experimental Apparatus. The electrochemical experiments were carried out with a frequency response analyzer (FRA, Model 7200 AMEL) along with a potentiostat (AMEL 7050) or with an Autolab 320 potentiostat with FRA module (Metrohm, Switzerland).

Two kinds of electrochemical cells were used for the experiments. A three-electrode cell (beaker cell BC) was used for most of the electrochemical runs and for the main electrochemical characterisation tests. In the BC the TiO_2 sample was the working electrode (WE); the surface was partially shielded to have nominal electrode area of 1 cm^2. A platinum grid and a saturated calomel electrode (SCE) were the counter (CE) and the reference electrodes (RE), respectively; all the values of potential in the text are referred to SCE.

Experiments were also performed in a two electrodes thin gap cell (TGC): in this case the TiO_2 sample (WE) was directly faced to the counter electrode (CE), in a filter press configuration, with an active anode surface of 0.4 cm^2.

The counter electrode was a commercial fluorine-doped tin oxide (FTO, supplied by SOLARONIX) over which nanoparticles of Pt were deposited in a very thin film so that the final surface remained optically transparent. A thin polymeric spacer (100 μm thickness) was interposed between WE and CE to avoid short-circuits and contain the electrolyte. The cell was sealed by clips.

2.3. Experimental Runs. Photo-currents tests were performed in 0.1 M KOH solution. The light source was a 300 W Xe lamp (Lot Oriel) equipped with an IR water-filter and with suitable optical filters to select the wavelength of 340, 365, 380, and 400 nm. Depending on the filter, the average light power (P) striking on the surface of the electrode ranged from 1.5 to 11 mW cm^{-2}. Preliminary potentiostatic runs were performed in order to individuate suitable potential values at which photocurrents measured at the different samples could be compared. As discussed below, a value of 1 V from the open circuit potential (OCV) resulted suitable for this comparison. The photocurrent values were calculated by subtracting the values obtained in the dark from those measured under irradiation.

Electrochemical Impedance Spectroscopy (EIS) measurements were performed in 0.1 M KOH at different bias potentials in a frequency range from 100 kHz to 0.1 Hz. In order to measure the faradaic impedance of the samples specific measurements were performed in an equimolar 5 mM ferro/ferricyanide solution with 0.1 M phosphoric buffer at pH = 7.

3. Results and Discussion

Figure 1 shows the SEM images of the electrodes: the ordered nanotubular structure of the NT and NTD electrodes is well evident: the mean diameter of the nanotubes is about 80–100 nm, the wall thickness is about 20 nm. The mean diameter of the nanoparticles in the decorated structures NTD and OCD is 20 nm.

Figure 2 shows an example of trend of the normalised currents as a function of the overpotential η (measured as difference between applied potential E_{app} and OCV), obtained at two different samples irradiated with 400 nm incident light. Depending on the samples the plateau of photocurrent saturation was well visible even at low overpotential, as in the case of the sample NTD in the figure; in other cases a higher overpotential had to be applied before achieving saturation. In order to make a comparison between photoactivity of all the samples an overpotential value of 1V was selected for the subsequent measurements, which resulted sufficient for the current at all the samples to be nearly independent from the applied potential.

Figure 3 shows the trend of photocurrents measured at η = 1 V and at different wavelengths at the four samples. The data were normalised with respect to the effective power (P) of the incident light, to account for the difference due to the filters of the Xe lamp. As we expected, the best efficiencies were obtained in the range of the lower wavelengths, indicating that only the most energetic light is able to activate the generation of charge in the structures of all the samples. Moreover, all data demonstrate the effectiveness of the decoration process (DP), which resulted in an increase of the photocurrent values: this is particularly evident in the range of the low wavelengths, whereas no appreciable difference is noticeable at the highest investigated wavelength (430 nm): in this case, due to the low absolute values of the currents measured, the comparison between the relevant behaviours tends to lose the significance. Further considerations can be derived from data related to the gain in photocurrent obtained with the decoration process. With this aim, data in the inset are shown in terms of the ratio γ between photocurrents measured at decorated and not-decorated samples ($\gamma = I_D/I$). As we can note γ was different for OC and NT samples, being higher for the compact oxides rather than for the nanotubes; moreover, for the two kinds of samples, the maximum gain in photocurrent due to the decoration occurs at different wavelength: the highest value of γ = 13.75 is obtained at 380 nm for compact oxides, while a value of 9.6 represents the best gain in performance achieved at 400 nm in the case of nanotubular samples. This trend could indicate that the gain in efficiency is not only due to the higher surface of the decorated samples, and it suggested us further investigation to individuate possible other influent factors responsible for the observed trend.

In this context the samples were characterised by impedance spectroscopy in the dark at different potential either in 0.1 M KOH or in ferro/ferricyanide.

Figure 4(a) presents the Nyquist plot of NT sample in KOH: a great dependence of data on the potential can be observed. The impedances are quite low in the range of potential in which the semiconductor is in accumulation regime, and then they increase when measurements are done in the potential at which the space charge of the semiconductor becomes depleted.

The Bode diagrams is also worth to be considered (Figures 4(b)-4(c)): in the phase diagrams obtained at the more negative potentials two processes are evidenced at the highest and the lowest frequency, but when we move to more positive potentials a new time constant appears which may be attributed to the depletion of the space charge of the semiconductor.

If the analogous data for NTD sample are considered, (Figure 5) lower values of the impedances in the Nyquist plot, with values of $Z''Z'$ within the range 320–60 Ohm, can be observed. Moreover, data show a lower dependence on the potential.

On the basis of the results from EIS measurements carried out in the dark also the Mott Schottky (MS) analysis was performed. The imaginary component of impedance Z'' measured at each frequency is used in this analysis to evaluate the space charge capacitance as $C = 1/2\pi f Z''$, and its trend with potential allows to derive information on the semiconductor behaviour. In particular, for an ideal capacitive behaviour of a *n-type* semiconductor a positive slope of the linear trend of $1/C^2$ versus V is obtained, and flat band potential and donor concentration of the semiconductor can be derived from this trend. It should be noted that MS analysis is strictly applicable to regular compact oxides and under depletion conditions of the space charge layer. However, it

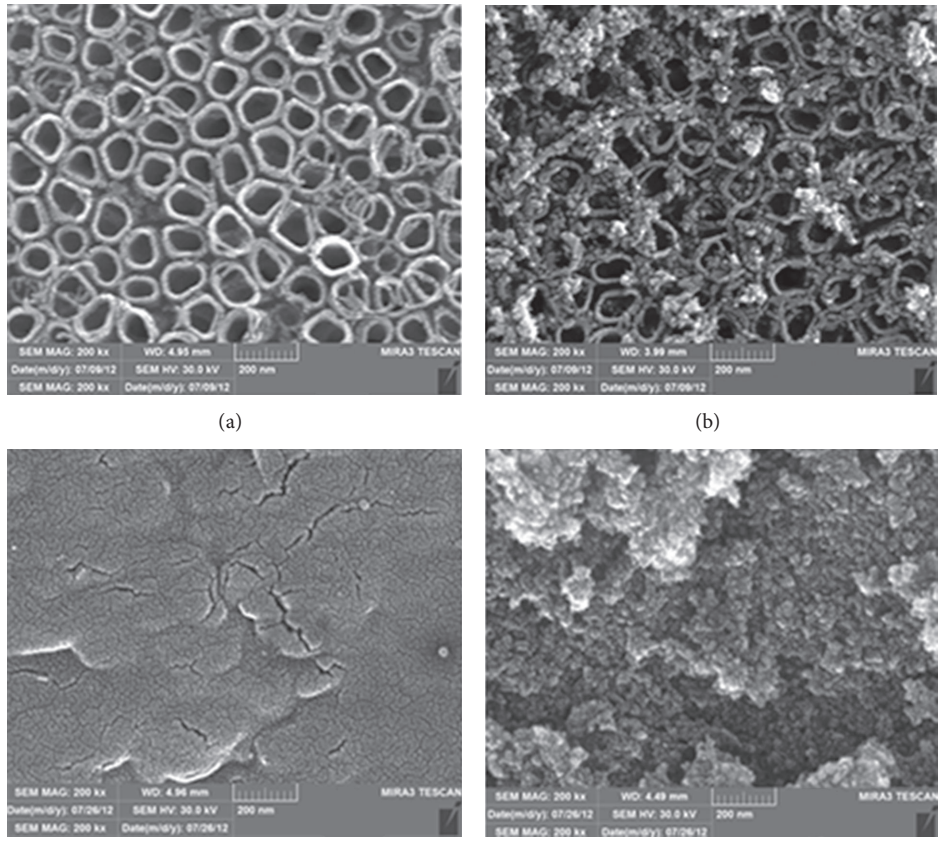

Figure 1: SEM images of the anodes utilised: nanotubular TiO_2 (NT) (a); nanotubular TiO_2 decorated (NTD) (b); compact oxides (OC) (c); compact oxide decorated (OCD) (d).

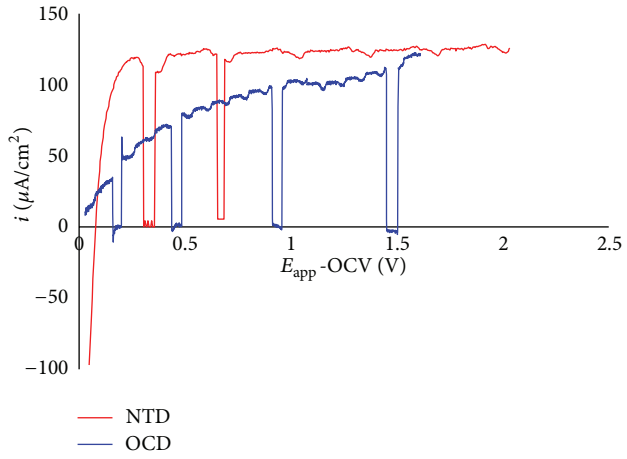

Figure 2: Trend of current density as a function of the overpotential, obtained at NTD (red curve) and OCD (blue curve) in 0.1 M KOH solution under irradiation of a Xenon lamp equipped with a 400 nm filter. The points of light-off are well evidenced in the curves.

is often applied also to irregular geometries with porous surfaces as well as to nanotubular layers [36].

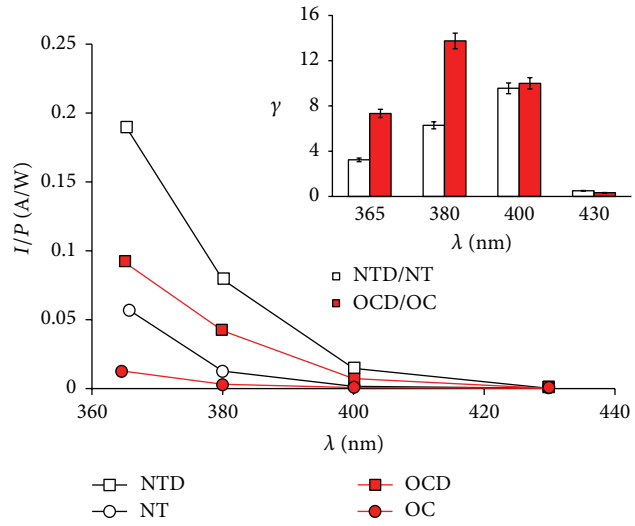

Figure 3: Values of photocurrent, normalized with respect to the power of incident light, obtained at different wavelengths with different samples, during potential steps at 1 V from the OCV. The inset shows the performance gain γ evaluated as ratio between the current values obtained with decorated and not decorated samples ($\gamma = I_D/I$).

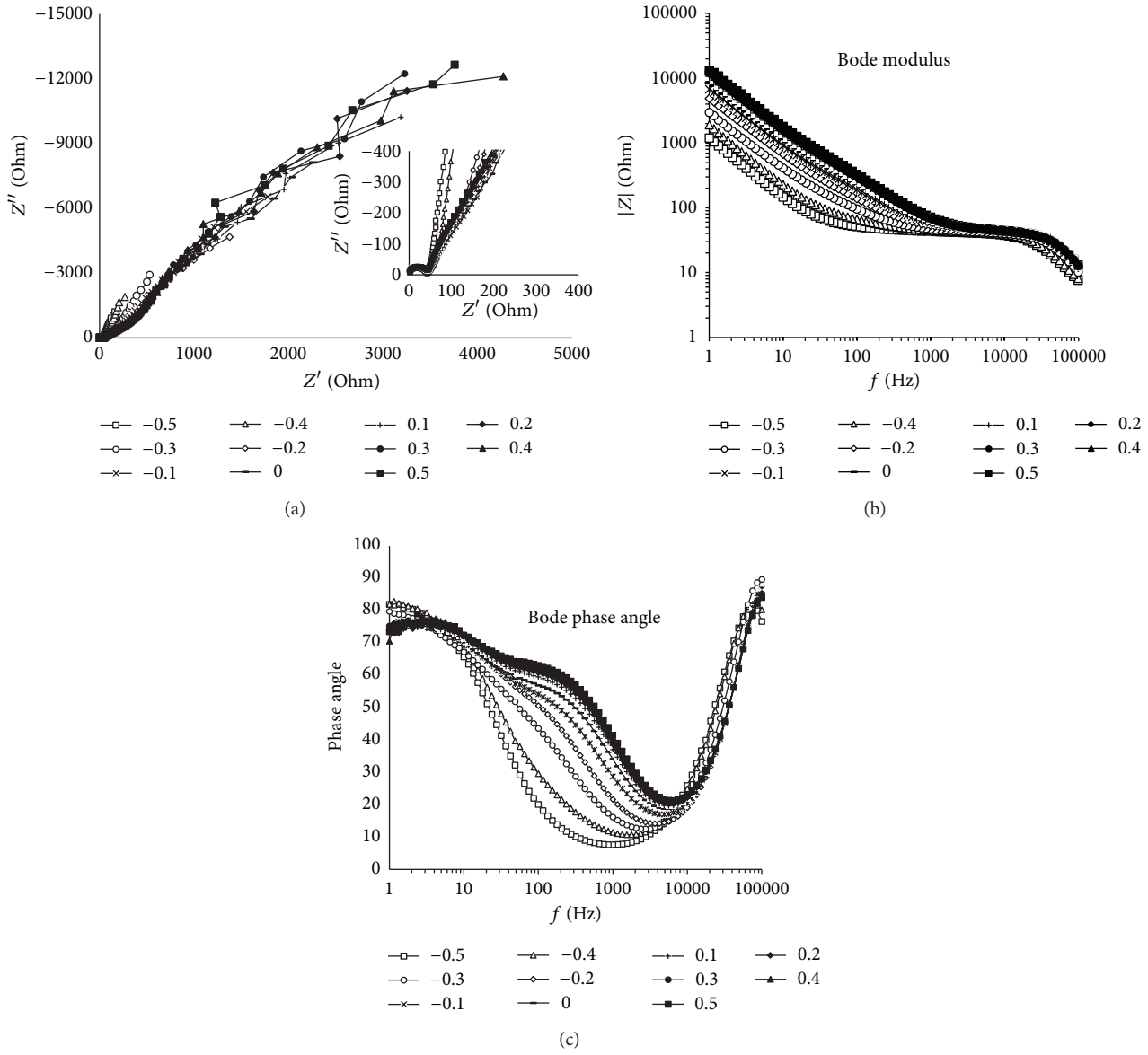

Figure 4: EIS spectra of NT sample, recorded at different bias potentials in 0.1 M KOH.

Figure 6 shows the MS data for the sample NTD: a strong spreading of data with the frequency was obtained, as we expected due to the high porosity of the sample. We also can note at the highest frequencies (Figure 6, $f < 100{,}000$ Hz), the positive slope of the linear part of the curves, as it is due to an *n-type* semiconductor. But if we observe the data at lower range of frequency (Figure 6, $f < 25{,}000$ Hz), the trend changes and also a change in the slope appears (Figure 6, $f < 3{,}000$ Hz).

A different behaviour was observed for the NT sample (Figure 7): also in this case a high dispersion of data can be observed, but the change in the slope did not occur, even at very low frequency region (Figure 7, $f < 100$ Hz). This difference between NT and NTD samples indicates a possible change in the distribution of the sites of different nature involved in the charge transfer process in the semiconductor [37].

Further information was obtained from the results of EIS measurements in ferro/ferricyanide solution. This couple is a well-known reversible redox couple which is generally used to measure the faradaic impedance, that is, the ability of the solid/solution interface in the charge transfer process.

The relevant impedance spectra of NT and NTD samples are shown in Figure 8: the diameter of the semicircle of the NTD spectrum is about 5 times lower than that related to the NT. Since the diameter of the semicircle in the Nyquist plot can be directly related to the charge transfer resistance, this result indicates that the DP generated new sites in the structure, which favour the charge transfer process at the solid/liquid interface.

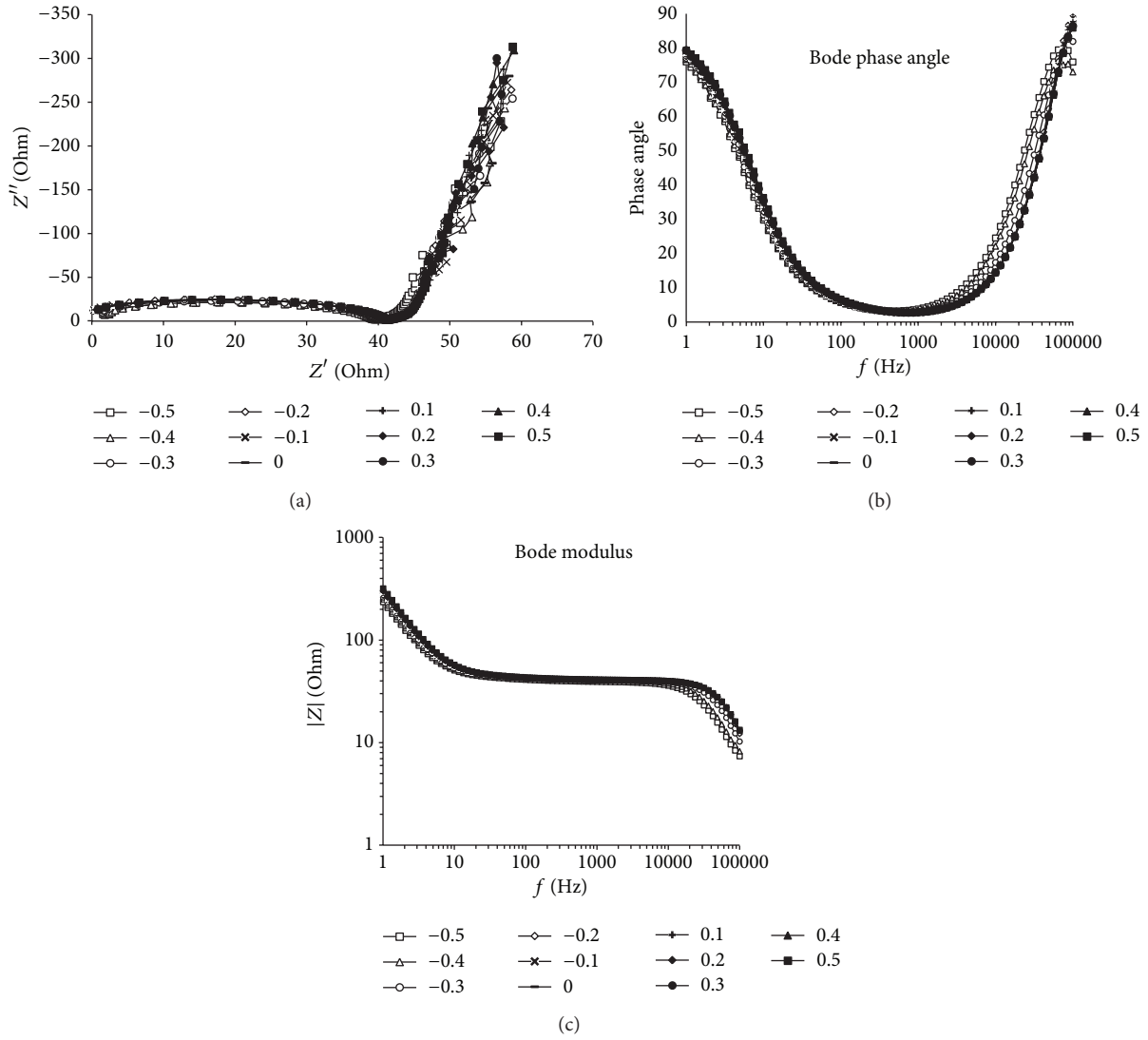

Figure 5: EIS spectra of NTD sample, recorded at different bias potentials in 0.1 M KOH.

The results obtained can be explained considering the nature of the defects which determine the behaviour of TiO_2. As it is well known the photoactivity of titania is strictly connected to the defects which are originated in its structure: TiO_2 would not be active if it was not defective [38–40]. In particular, to describe the photocatalytic activity of TiO_2, we should consider the oxygen vacancies, the Ti vacancies, and the Ti interstitials [41]. The oxygen vacancies or the interstitial Ti, which by their nature are donors, correspond to energetic levels near to the conduction band [42]. It is generally accepted in the literature that in a nanotubular structure this kind of defects is mainly concentrated at the walls of nanotubes. The Ti vacancies are acceptors and correspond to energetic levels near to the valence band. These defects are mainly located in the bulk material, such as in the compact layer which has not been interested by tubes formation [37, 43].

All the above results could indicate that the decoration process allowed generating new interphases at which the concentration of superficial states is very high: a high concentration of O_2 vacancies may be generated at the grain boundaries of the nanostructured particles. This results in a high conductivity, a high concentration of donors in the space charge, and in turn the low dependency observed of the data on the potential (Figure 5). Their effect is so important that the effect of the bulk sites is shielded: we can see the contribution of the bulk sites only by perturbing the system with very low frequencies (see Figure 6).

The performances of the samples have also been tested in a TGC: the values of photocurrent obtained at 365 and 400 nm are reported in Figures 9(a) and 9(b), respectively, along with those obtained in the BC for comparison. As can be seen, also in this case the DP led to higher values of photocurrent.

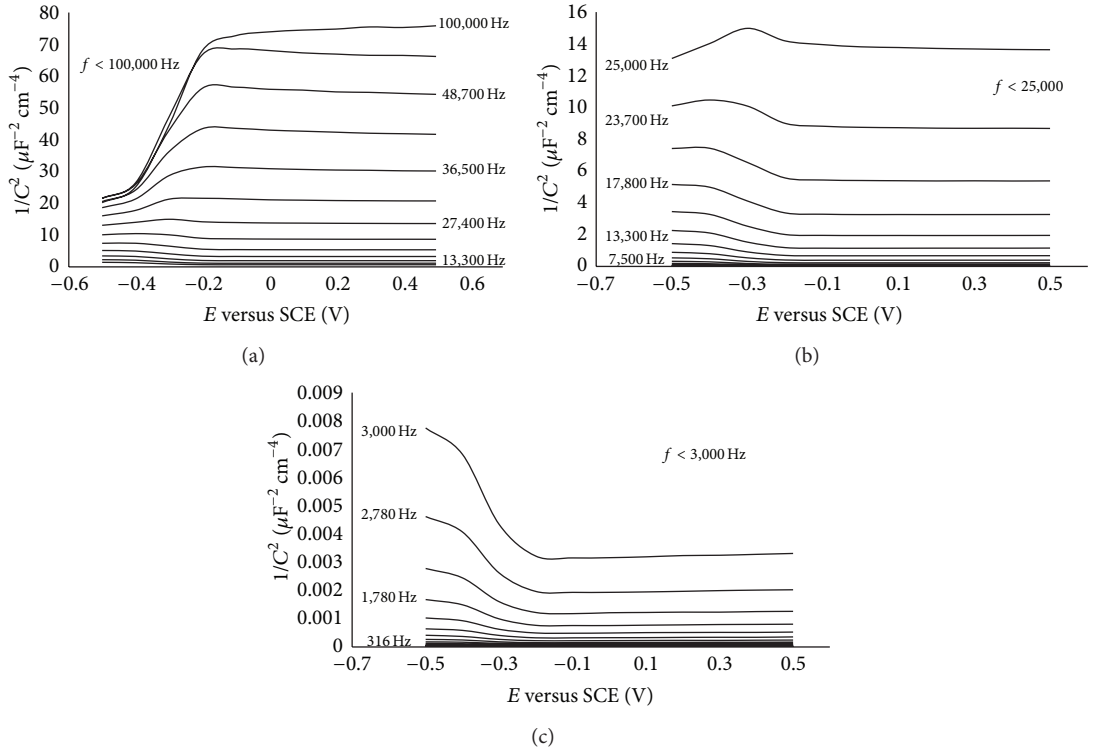

Figure 6: Mott Schottky plots of NTD sample in different ranges of frequencies.

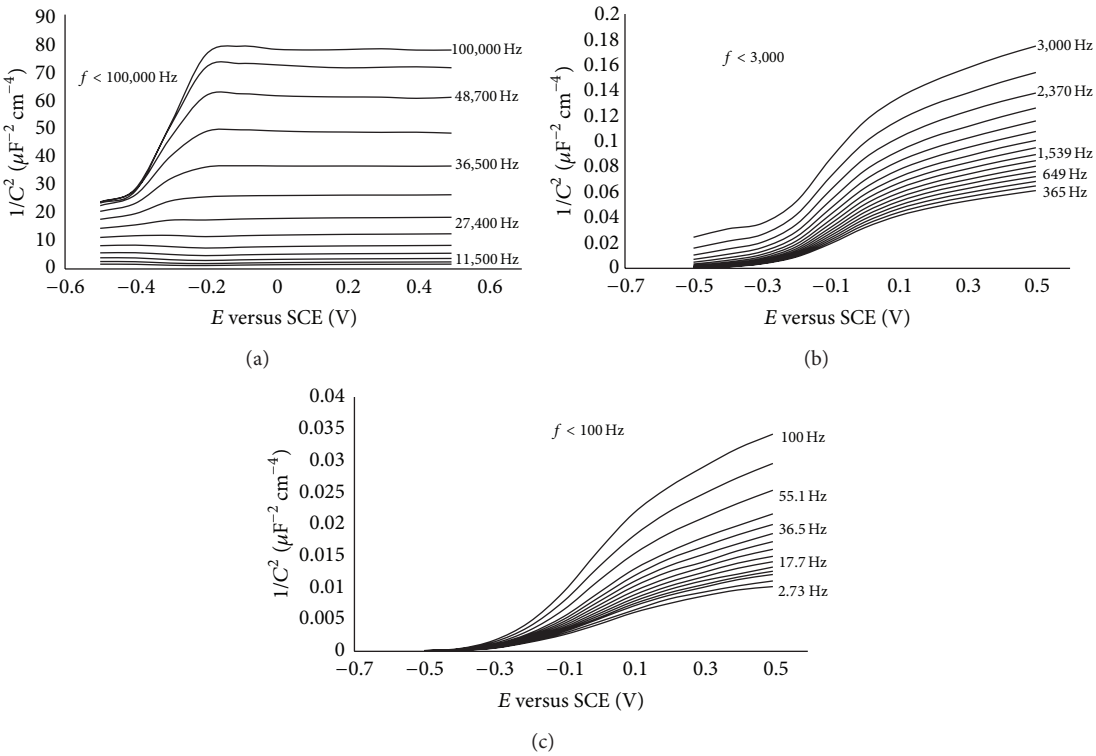

Figure 7: Mott Schottky plots of NT sample in different ranges of frequencies.

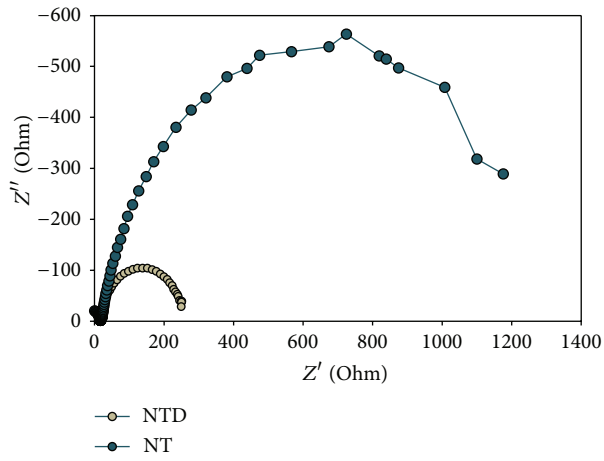

Figure 8: Nyquist plot of EIS recorded at the OCV in 5 mM ferro/ferricyanide at pH = 7 with different samples.

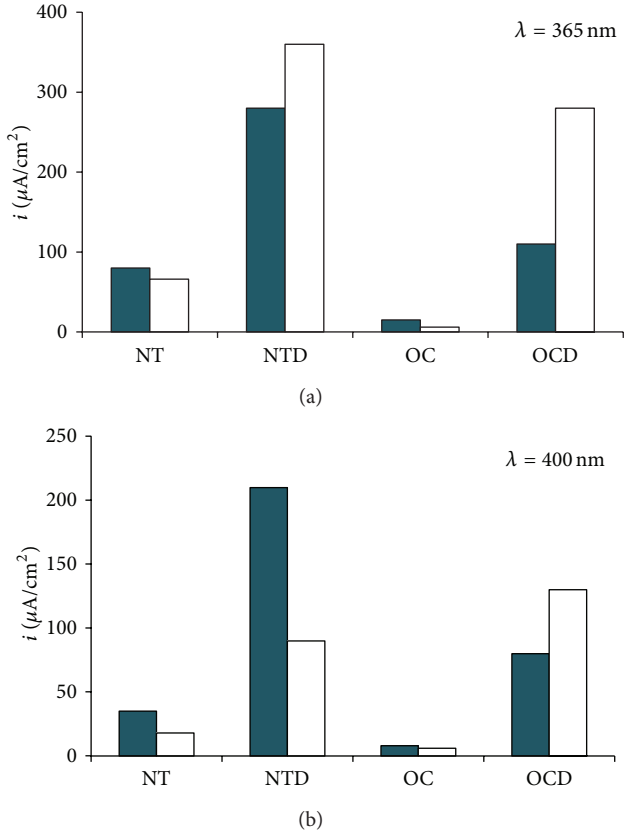

Figure 9: Values of photocurrent obtained at 365 nm (a) and 400 nm (b) in the BC (full bars) and in TGC (empty bars).

In order to explain the combined effect *cell configuration-wavelength* in Figure 9, the previous considerations have to be completed with the effect of the radiation on defects, as well as with the relevance of the different phenomena involved in the whole process of charge transfer across the cell. Considering that the main steps of the process are the charge transfer in the electrolyte/electrode interfaces, in the electrolyte and in the solid film, the process can then roughly sketched as a three in series impedances: corresponding to the solution (Z_s), the solid film (Z_f), and the solid/liquid interface. A further element should be considered in the TGC, due to the presence of the counter electrode/electrolyte interface. Passing from BC to TGC is expected to result in a significant decrease of the diffusive resistance, since the interelectrode gap of TGC is in the order of magnitude of a diffusion layer [35]. As stated above a high concentration of highly conductive superficial sites is present in decorated structures (NTD and OCD) due to the DP. Depending on the wavelength of the incident light, these sites may be more or less involved in the process. Actually, the lower the wavelength, the higher the energy; at the same time, the absorption coefficient of the light increases as the wavelength decreases and in turn a lower penetration path of the radiation is obtained at the lowest wavelength.

At 365 nm the light is energetic but it could be not enough penetrating, so that superficial states are mostly involved in the response, while bulk defects are not significantly interested. The performance is mainly determined by the contribution of the tube walls and of the nanoparticles distributed on them. The high conductivity of the decorated samples (either NTD or OCD) makes the photocurrent at the electrode sufficiently high itself, so that the solution impedance Z_s limits the process. This may justify the results in Figure 9(a): passing from the BC to the TGC results in a decrease of the total impedance, and this in turn increases the performance of the process, because it allows reducing the limiting step (Z_s).

This effect is not evident in NT and OC samples: the slight lower performances obtained at TGC may be due to the presence of the counter electrode/electrolyte interface [35] which becomes more significant when the sample presents lower conductivity as in the case of NT and OC.

When the wavelength of 400 nm is considered (Figure 9(b)), we observe a different behaviour. The energy of radiation is lower, and the absolute values of photocurrent measured are lower than in the previous case. The radiation (more penetrating) is able to involve also the bulk sites, mainly concentrated in the compact layer of the structure, and their response may be relevant and comparable to that of superficial states. A different trend of the results is obtained at this wavelength depending on the samples: the accessibility of the compact layer of the structures becomes a crucial point. Actually, the results in Figure 9(b) indicate that the performance of NT is poorly affected by the cell configuration: in both the configurations the electrolyte is able to easily contact walls and bottom of the tubes so that bulk and superficial states may give their contributions to the current. Also in this case the low decrease of the photocurrent, passing from the BC to the TGC, may be attributed to phenomena related to the counter electrode.

A strong difference in the performance of the two cell configurations is instead obtained when NTD sample is considered. In this case the presence of the nanoparticles may limit the accessibility of the electrolyte to the bottom of NTs (compact layer), and in turn the contribution of bulk sites is excluded. This effect is much more evident at the TGC

where only a thin layer of electrolyte may be not sufficient to guarantee a suitable interphase solid/electrolyte.

When compact oxides are considered, at the wavelength of 365 nm we observe (Figure 9(a)) an analogous behaviour as in the case of NT structures: the removal of the Z_s component leads to high photocurrents at TGC rather than at BC. However, differently from what we observed at NT structures, in the case of OCD, the performance at TGC remains better than at BC also at 400 nm (Figure 9(b)). The results could be justified by considering that in this case the availability of the bulk sites is not hindered, since the compact layer of the oxide is directly connected to the particles of the decoration, so that eliminating the solution does not compromise the global efficiency but rather leads to a beneficial effect in terms of reduced global impedance.

4. Conclusions

The photo electrochemical performances of titanium oxide based anodes were investigated in this work. The presence of TiO_2 nanoparticles on the surface of the titania anodes generally led to higher values of photocurrent, which are correlated to a higher superficial area of the resulting samples, but also to a higher concentration of superficial states that confer high conductivity to the samples. A strong influence of the wavelength of the incident light was observed, and a singular combined effect *wavelength-cell configuration* has been evidenced. Results demonstrated that, depending on the cell configuration and on the wavelength of the irradiating light, the superficial and bulk sites may be involved in the process in different extent. The concentration of the two kinds of sites, as well as their accessibility by the electrolyte, resulted to be crucial in determining the final performance of the samples.

Acknowledgments

The authors wish to thank Pablo Ampudia for his support in the experimental work.

References

[1] M. Momirlan and T. N. Veziroglu, "Current status of hydrogen energy," *Renewable & Sustainable Energy Reviews*, vol. 6, no. 1-2, pp. 141–179, 2002.

[2] K. Nakata and A. Fujishima, "TiO_2 photocatalysis: design and applications," *Journal of Photochemistry and Photobiology C*, vol. 13, no. 3, pp. 169–189, 2012.

[3] A. L. Stroyuk, V. V. Shvalagin, A. E. Raevskaya, A. I. Kryukov, and S. Y. Kuchmii, "Photochemical formation of semiconducting nanostructures," *Theoretical and Experimental Chemistry*, vol. 44, no. 4, pp. 205–231, 2008.

[4] W. Zhou, H. Liu, R. I. Boughton et al., "One-dimensional single-crystalline Ti-O based nanostructures: properties, synthesis, modifications and applications," *Journal of Materials Chemistry*, vol. 20, no. 29, pp. 5993–6008, 2010.

[5] Y. Lan, X. Gao, H. Zhu et al., "Titanate nanotubes and nanorods prepared from rutile powder," *Advanced Functional Materials*, vol. 15, no. 8, pp. 1310–1318, 2005.

[6] M. Ye, C. Chen, M. Lv, D. Zheng, W. Guo, and C. Lin, "Facile and effective synthesis of hierarchical TiO_2 spheres for efficient dye-sensitized solar cells," *Nanoscale*, vol. 5, no. 14, pp. 6577–3583, 2013.

[7] P.-L. Kuo, T.-S. Jan, C.-H. Liao, C.-C. Chen, and K.-M. Lee, "Syntheses of size-varied nanorods TiO_2 and blending effects on efficiency for dye-sensitized solar cells," *Journal of Power Sources*, vol. 235, pp. 297–302, 2013.

[8] G. He, Y. Cai, Y. Zhao et al., "Electrospun anatase-phase TiO_2 nano fibers with different morphological structures and speciffic surface areas," *Journal of Colloid and Interface Science*, vol. 398, pp. 103–111, 2013.

[9] S. Palmas, A. Da Pozzo, F. Delogu, M. Mascia, A. Vacca, and G. Guisbiers, "Characterization of TiO_2 nanotubes obtained by electrochemical anodization in organic electrolytes," *Journal of Power Sources*, vol. 204, pp. 265–272, 2012.

[10] S. Palmas, A. da Pozzo, M. Mascia, A. Vacca, R. Matarrese, and I. Nova, "Photo-electrochemical behavior at different wavelengths of electrochemically obtained TiO_2 nanotubes," *Journal of Applied Electrochemistry*, vol. 42, no. 9, pp. 745–751, 2012.

[11] S. Sreekantan, K. A. Saharudin, Z. Lockman, and T. W. Tzu, "Fast-rate formation of TiO_2 nanotube arrays in an organic bath and their applications in photocatalysis," *Nanotechnology*, vol. 21, no. 36, Article ID 365603, 2010.

[12] M. Park, A. Heo, E. Shim, J. Yoon, H. Kim, and H. Joo, "Effect of length of anodized TiO_2 tubes on photoreactivity: photocurrent, Cr(VI) reduction and H_2 evolution," *Journal of Power Sources*, vol. 195, no. 15, pp. 5144–5149, 2010.

[13] H. Ishihara, J. P. Bock, R. Sharma et al., "Electrochemical synthesis of titania nanostructural arrays and their surface modification for enhanced photoelectrochemical hydrogen production," *Chemical Physics Letters*, vol. 489, no. 1–3, pp. 81–85, 2010.

[14] R. Chauhan, R. Kushwaha, and L. Bahadur, "Highly effficient dye-sensitized solar cell developed by using sheet like TiO_2 prepared by a novel route," *Materials Chemistry and Physics*, vol. 139, pp. 525–530, 2013.

[15] C. Bae, Y. Yoon, W.-S. Yoon, J. Moon, J. Kim, and H. Shin, "Hierarchical titania nanotubes with self-branched crystalline nanorods," *ACS Applied Materials & Interfaces*, vol. 2, no. 6, pp. 1581–1587, 2010.

[16] M. Ye, C. Chen, M. Lv, D. Zheng, W. Guo, and C. Lin, "Facile and effective synthesis of hierarchical TiO_2 spheres for efficient dye-sensitized solar cells," *Nanoscale*, vol. 5, pp. 6577–6583, 2013.

[17] T.-D. Nguyen-Phan, E. J. Kim, S. H. Hahn, W.-J. Kim, and E. W. Shin, "Synthesis of hierarchical rose bridal bouquet- and humming-top-like TiO_2 nanostructures and their shape-dependent degradation efficiency of dye," *Journal of Colloid and Interface Science*, vol. 356, no. 1, pp. 138–144, 2011.

[18] J. Zhou, G. Zhao, B. Song, and G. Han, "Solvent-controlled synthesis of three-dimensional TiO_2 nanostructures via a one-step solvothermal route," *CrystEngComm*, vol. 13, no. 7, pp. 2294–2302, 2011.

[19] W. Y. Cheng, J. R. Deka, Y. C. Chiang, A. Rogeau, and S. Y. Lu, "One-step, surfactant-free hydrothermal method for syntheses of mesoporous TiO_2 nanoparticle aggregates and their applications in high efficiency dye-sensitized solar cells," *Chemistry of Materials*, vol. 24, no. 16, pp. 3255–3262, 2012.

[20] J.-H. Lee, "Gas sensors using hierarchical and hollow oxide nanostructures: overview," *Sensors and Actuators B*, vol. 140, no. 1, pp. 319–336, 2009.

[21] J. Yu, W. Liu, and H. Yu, "A one-pot approach to hierarchically nanoporous titania hollow microspheres with high photocatalytic activity," *Crystal Growth & Design*, vol. 8, no. 3, pp. 930–934, 2008.

[22] X. Bai, B. Xie, N. Pan, X. Wang, and H. Wang, "Novel three-dimensional dandelion-like TiO_2 structure with high photocatalytic activity," *Journal of Solid State Chemistry*, vol. 181, no. 3, pp. 450–456, 2008.

[23] L. Li, Z. Zhou, J. Lei, J. He, S. Wu, and F. Pan, "Facile fabrication of a dual hierarchical TiO_2 nanostructure," *Materials Letters*, vol. 68, pp. 290–292, 2012.

[24] Y. Tang, P. Wee, Y. Lai et al., "Hierarchical TiO_2 nanoflakes and nanoparticles hybrid structure for improved photocatalytic activity," *The Journal of Physical Chemistry C*, vol. 116, no. 4, pp. 2772–2780, 2012.

[25] G. Li, H. Zhang, J. Lan et al., "Hierarchical hollow TiO_2 spheres: facile synthesis and improved visible-light photocatalytic activity," *Dalton Transactions*, vol. 42, no. 24, pp. 8541–8544, 2013.

[26] D. Deng and J. Y. Lee, "Hollow core-shell mesospheres of crystalline SnO_2 nanoparticle aggregates for high capacity Li+ ion storage," *Chemistry of Materials*, vol. 20, no. 5, pp. 1841–1846, 2008.

[27] A. Hu, C. Cheng, X. Li et al., "Two novel hierarchical homogeneous nanoarchitectures of TiO_2 nanorods branched and p25-coated TiO_2 nanotube arrays and their photocurrent performances," *Nanoscale Research Letters*, vol. 6, no. 1, p. 91, 2011.

[28] M. A. Henderson, "A surface science perspective on TiO_2 photocatalysis," *Surface Science Reports*, vol. 66, no. 6-7, pp. 185–297, 2011.

[29] L. Xiang, X. Zhao, C. Shang, and J. Yin, "Au or Ag nanoparticle-decorated 3D urchin-like TiO_2 nanostructures: synthesis, characterization, and enhanced photocatalytic activity," *Journal of Colloid and Interface Science*, vol. 403, pp. 22–28, 2013.

[30] L. Pan, J.-J. Zou, S. Wang et al., "Quantum dot self-decorated TiO_2 nanosheets," *Chemical Communications*, vol. 49, no. 59, pp. 6593–6595, 2013.

[31] M. Jankulovska, I. Barceló, T. Lana-Villarreal, and R. Gómez, "Improving the photoelectrochemical response of TiO_2 nanotubes upon decoration with quantum-sized anatase nanowires," *The Journal of Physical Chemistry C*, vol. 117, no. 8, pp. 4024–4031, 2013.

[32] S. Palmas, A. M. Polcaro, J. R. Ruiz et al., "Effect of the mechanical activation on the photoelectrochemical properties of anatase powders," *International Journal of Hydrogen Energy*, vol. 34, no. 24, pp. 9662–9670, 2009.

[33] S. Palmas, A. da Pozzo, M. Mascia, A. Vacca, and R. Matarrese, "Investigation on the adsorption and photooxidation of glycerol at TiO_2 nanotubular arrays," *International Journal of Photoenergy*, vol. 2012, Article ID 914757, 7 pages, 2012.

[34] S. Palmas, A. da Pozzo, M. Mascia et al., "Effect of the preparation conditions on the performance of TiO_2 nanotube arrays obtained by electrochemical oxidation," *International Journal of Hydrogen Energy*, vol. 36, no. 15, pp. 8894–8901, 2011.

[35] A. Attour, S. Rode, A. Ziogas, M. Matlosz, and F. Lapicque, "A thin-gap cell for selective oxidation of 4-methylanisole to 4-methoxy-benzaldehyde-dimethylacetal," *Journal of Applied Electrochemistry*, vol. 38, no. 3, pp. 339–347, 2008.

[36] P. Pu, H. Cachet, and E. M. M. Sutter, "Electrochemical impedance spectroscopy to study photo-induced effects on self-organized TiO_2 nanotube arrays," *Electrochimica Acta*, vol. 55, no. 20, pp. 5938–5946, 2010.

[37] S. Palmas, A. M. Polcaro, J. R. Ruiz, A. da Pozzo, M. Mascia, and A. Vacca, "TiO_2 photoanodes for electrically enhanced water splitting," *International Journal of Hydrogen Energy*, vol. 35, no. 13, pp. 6561–6570, 2010.

[38] J. Nowotny, T. Bak, M. K. Nowotny, and L. R. Sheppard, "Titanium dioxide for solar-hydrogen II. Defect chemistry," *International Journal of Hydrogen Energy*, vol. 32, no. 14, pp. 2630–2643, 2007.

[39] J. Nowotny, T. Bak, M. K. Nowotny, and L. R. Sheppard, "Titanium dioxide for solar-hydrogen III: kinetic effects at elevated temperatures," *International Journal of Hydrogen Energy*, vol. 32, no. 14, pp. 2644–2650, 2007.

[40] J. Nowotny, T. Bak, M. K. Nowotny, and L. R. Sheppard, "Titanium dioxide for solar-hydrogen IV. Collective and local factors in photoreactivity," *International Journal of Hydrogen Energy*, vol. 32, no. 14, pp. 2651–2659, 2007.

[41] V. K. Mahajan, M. Misra, K. S. Raja, and S. K. Mohapatra, "Self-organized TiO_2 nanotubular arrays for photoelectrochemical hydrogen generation: effect of crystallization and defect structures," *Journal of Physics D*, vol. 41, no. 12, Article ID 125307, 2008.

[42] G. Mattioli, P. Alippi, F. Filippone, R. Caminiti, and A. Amore Bonapasta, "Deep versus shallow behavior of intrinsic defects in rutile and anatase TiO_2 polymorphs," *The Journal of Physical Chemistry C*, vol. 114, no. 49, pp. 21694–21704, 2010.

[43] M. Zlamal, J. M. Macak, P. Schmuki, and J. Krýsa, "Electrochemically assisted photocatalysis on self-organized TiO_2 nanotubes," *Electrochemistry Communications*, vol. 9, no. 12, pp. 2822–2826, 2007.

The Scientific World Journal

Hindawi Publishing Corporation
http://www.hindawi.com

Volume 2013